Deep eutectic solvents and traditional refrigerants in absorption refrigeration cycles using molecular approaches

Carlos Imas[a], Johan González[a], Fèlix Llovell[b], José Matías Garrido[c], Héctor Quinteros-Lama[a,*]

[a]*Departamento de Tecnologías Industriales, Faculty of Engineering, Universidad de Talca. Merced 437, Curicó, Chile*
[b]*Department of Chemical Engineering, ETSEQ, Universitat Rovira i Virgili, Avda Països Catalans 26, 43007 Tarragona, Spain*
[c]*Departamento de Ingeniería Química, Faculty of Engineering, Universidad de Concepción, Concepción, Chile*

Abstract

Absorption Refrigeration Cycles (ARC) represent a sustainable technology capable to effectively produce cold with a modest energy consumption from the use of waste heat or renewable sources. However, the right choice of the working fluid pair absorbent-refrigerant is essential for a proper working of the system. This contribution is devoted to analyse the performance of an ARC with a heat exchanger using a wide variety of refrigerants in combination with selected deep eutectic solvents (DES) as absorbents. Three choline chloride-based and one ionic liquid (IL)-based DESs as absorbers are combined with sixteen different refrigerants, including hydrocarbons, hydrofluorocarbons and hydrofluoroolefins.The PC-SAFT equation of state is employed to assess the thermophysical properties of these compounds under the operating conditions of the cycle. Accurate modelling of the absorption cycle has revealed that the phase behaviour of the working mixture, especially at high DES concentrations, significantly constrains the temperature and pressure range within which the cycle can operate. Moreover, idealised models of absorption cycles are insufficient for accurately representing the capabilities and limitations of these systems, mainly when dealing with complex working mixtures. From the sixty-four working pair mixtures, only eighteen are suitable for ARCs based on technical and thermodynamics criteria. Nevertheless, most mixtures exhibit modest coefficient of performance (COP) efficiencies. The use of additional Key Performance Indicators related to environmental and safety constraints is added to COP to perform a holistic analysis, establishing a ranking of the best options. Preliminary results indicate that the IL-based DES, in combination with R227ea and R236ea provide the best performance among all studied systems.

Keywords: Absorption refrigeration cycle; Deep eutectic solvents (DES); PC-SAFT; Climate change.

1. Introduction

The current worldwide environmental concerns are mostly focused on the adverse repercussions triggered by the accumulation of Greenhouse Gases (GHGs) in the atmosphere. Human activities have significantly altered the natural and necessary greenhouse effect exhibited by the planet, leading to an excessive global warming and one of its most undesirable outcomes: the accelerated progression of climate change [1]. The Paris Agreement of 2015 stands as one of the most significant international accords aimed at creating effective tools to reduce greenhouse gas emissions. It established a target of limiting the increase in global temperature to 2°C above pre-industrial levels, with a strong commitment not to surpass 1.5°C. Unfortunately, the 1.5 °C goal is likely to be reached between 2030 and 2052 if the temperature keeps increasing at the current rate. According to the "*Sustainable Development Goals Report*" from 2021 and its "*Goal 13*" related to climate action, it is necessary to decrease the anthropogenic CO_2 emissions by at least 45 % before 2030 compared with 2010 levels and 100 % before 2050 to reach the 1.5 °C goal [2]. Practical actions to achieve these goals consists of abolishing coal as an energy source, increasing the investment in renewable energy, and reducing and recycling global warming gases [3–7].

Apart from carbon dioxide, other GHGs play an important role in the context of global warming. In particular, the effect of the so-called fluorinated gases (F-gases) is remarkable. F-gases constitute several families of compounds, including chlorofluorocarbons (CFCs) [8], hydrofluorocarbons (HFCs) [9, 10] and hydroflyorolefins (HFOs), which have been or are currently used in refrigeration, low-temperature power generation [6, 11], medicine [12], electronics [13], or as a solvent in the chemical industry [14]. While chlorofluorocarbons were banned from production due to their elevated ozone depletion potential (ODP), HFCs took the leading role in replacing the CFCs in all their applications [15]. For that reason, HFC production has constantly increased in the last decades in contrast with other GHGs, such as CO_2, whose emissions have been reduced because of new regulations and technological improvements [16].

*Corresponding author. hquinteros@me.com

However, the high Global Warming Potential (GWP) of most HFCs pushes towards its progressive reduction and substitution. Notably, hydrofluorooleofins (HFO), also called fourth-generation refrigerants, are one of the more promising replacement alternatives in the working fluid refrigeration or energy production areas [17–20]. They have lower GWP than HFCs and shorter life in the atmosphere. In this manner, HFOs are gaining prominence in vapour compression refrigeration (VCR) and organic Rankine cycle (ORC) systems [21–23].

An alternative to vapour compression technology is absorption refrigeration, which considers absorption equipment replacing the compressor [24]. The absorption technology is a promising alternative because it can use low-temperature sources to produce cold [25, 26]. However, these systems have limitations such as crystallisation [26], low performance [27–29], and the use of additional equipment to ensure the separation [30]. The basic configuration comprises an absorber, a pump, a generator, and an expansion valve. To a lesser extent than VCRs, this equipment utilises electrical energy to create a pressure difference and relies on a thermal energy source to separate the refrigerant from the absorbent.

Absorption refrigeration cycle systems (ARCs) are used in applications such as pre-cooling [31], as a complement of cogeneration [32], trigeneration [33], as well as integrated with VCR systems [34]. This latter application combines refrigerant and absorbent as working fluid pairs, being water/LiBr, for cooling above 0 °C, and NH_3/water for cooling below 0 °C the most common ones. However, these systems are not free of serious drawbacks related to corrosion, crystallisation, and low performance as a result of high viscosity and poor heat transfer. In this regard, new absorbents have been proposed, including aqueous solutions [35] and ionic liquids (ILs) [28]. In particular, ILs, commonly utilised as solvents, stand out for their low vapour pressure, tune-ability, chemical and thermal stability, and environmental compatibility [36, 37]. In fact, the use ILs in ARC systems has been studied in combination with ammonia [28, 38, 39], water [29], R1234ze(E) [40], and HFCs [41]. Furthermore, laboratory scale absorption cycles have been tested for R134a [42], and R134 [43], achieving maximum values for the cooling-to-total-energy (CE) of approximately 0.5 and 0.6, respectively.

Another family of interesting compounds concerns the use Deep Eutectic Solvents (DESs). DESs are mixtures of two or more substances, commonly solid at room temperature, that take on the roles of acceptor (HBA) and donor (HBD) in forming a hydrogen bond. The complex network of interactions results in a significant depression of the melting point of the mixture, far below from that of an ideal system. Firstly, described by Abbott et al. [44], their study has boomed in the last decade. In fact, research on DESs has delved into their physicochemical properties [45–47] as and practical applications [48–53], being proposed as successors of the ILs [54], based on their lower cost and good environmental characteristics. [55–57].

Focusing on the use of DES as absorbents in ARCs, Abedin et al. [58, 59] analysed DES-based absorption refrigeration cycles in two different studies. In the first one [37], the authors proposed mixtures between R134a as the refrigerant and three DESs as absorbents. All DESs had choline chloride (ChCl) as HBA and urea, glycerol, and ethylene glycol as HBDs. The authors applied the thermodynamic COSMO-RS model to determine the density and heat capacity in the proposed systems. The tested mixtures yielded a very wide range of efficiency between 1.4 and 99.1 %, based on the "waste-heat efficiency" criterium, which neglects the heat input of the generator equipment. Additional molecular dynamics simulations carried out by the authors revealed that the interactions between HBD of the DESs and R134a are weak and do not affect the solvation of the refrigerant. In the second study [59], R245fa, R1234zeE, and R1336mzzE were used as refrigerants, while ChCl-based DESs with ethylene glycol and levulinic acid as HBDs were chosen as absorbents. Using the same methodology above described, lower efficiencies were obtained. It is also worth to mention the work of Haghbakhsh et al. [36], presenting a complete energy and exergy analysis for an absorption system using ammonia as the refrigerant and three ChCl-based DES as absorbents, with urea, glycerol, and ethylene glycol as HBDs. The modelling is performed using the SRK-NRTL model, obtaining a coefficient of performance (COP) around 0.6. In this study, the absorber and the generator are critical equipment for the layout. Subsequently, Haghbakhsh et al. [60] proposed water as the refrigerant using the same set of DES chosen in the previous study [36]. In this case, the CPA EOS was applied to determine the thermophysical properties of the mixture and to simulate the cycle. The obtained COP of the aforementioned system lies between 0.7 and 0.8, concluding that the working pair water/DES have the potential to be used in ARCs.

This work aims to propose a theoretical methodology to analyse and systematise the applicability of DESs as potential absorbents in ARCs using the PC-SAFT equation of state (EOS), given its proven predictive capacity in complex mixtures. For this purpose, four different DESs, including three chlorine chloride based and one IL-based DES, are combined with a variety of refrigerants, involving hydrocarbons (HCs), HFCs and HFOs, to perform a complete study of sixty-four possible pairs. Based on a prescreening from basic technical requirements, thirty-six mixtures have been simulated and optimised in an absorption cycle in detail, under additional Key Performance Indicators.

The rest of the paper is organised as follows: next section is devoted to briefly discuss the theoretical details related to the PC-SAFT model and the ARC calculations. Section 3 includes a summary of the results of the different absorbent-refrigerant combinations, highlighting the most interesting insights. Finally, Section 4 summarises

our main findings.

2. Theoretical background

2.1. Absorption refrigeration cycle modelling

The absorption refrigeration cycle is a traditional configuration that lacks the compression stage. Analogously to a vapour-compression refrigeration system, the absorption process has a condenser and an evaporator stage. The compression state is replaced with the absorption of the refrigerant on a liquid and then pressurised in a pump. Subsequently, the mixture is separated into a refrigerant and an absorbent at a generator. Although the performance of this kind of equipment is typically lower than the vapour-compression systems, this configuration has the advantage of a low energy consumption. In addition, the required energy allows the use of solar power or hybrid systems for refrigeration, turning these cycles into a sustainable alternative.

Figure 1 shows a schematic representation of an absorption refrigeration cycle. The scheme of the process can be described in ten stages. A quasi-pure refrigerant saturated vapour (1) is mixed in the absorber with an absorbent-rich flow (7). Then, the result of this mixing process (2) is pumped towards the generator (3). A heat exchanger assists the generator in most absorption cycles and increases its performance, resulting in heated flow (4). The generator separates the mixture, where the refrigerant-rich phase is sent to the condenser (8), and the absorbent-rich flow is returned to the absorber (6) through an expansion valve (7). It is common to add a rectifier before the condenser to address any issues related with poor separation in the generator. Finally, the quasi-pure refrigerant is cooled, or eventually condensed (9), and expanded in a valve (10) to be fed again into the evaporator.

In an ideal case, the generator perfectly separates the refrigerant from the absorbent, resulting in the flows (8) and (5). Therefore, the blue lines in Fig. 1 represent the pure refrigerant, the crimson lines are pure absorbent, and the violet lines indicate mixture flows. However, at real conditions, the separation is incomplete. Consequently, the choice of the working fluid pairs is critical to approach this assumption.

Currently, several models for absorption cycles are available in the literature [24, 60–63]. Among them, it is worth to mention the notorious contributions of Yokozeki [24] and Raeissi [60]. In both cases, the flows linking the absorption and refrigeration parts are considered pure fluids, and the thermophysical properties are obtained through EOS.

One critical parameter for the analysis and modelling of this process is the flow ratio between the refrigeration section (flows (8), (9), (10), and (1)) and the absorption part of the cycle, f, which is given by

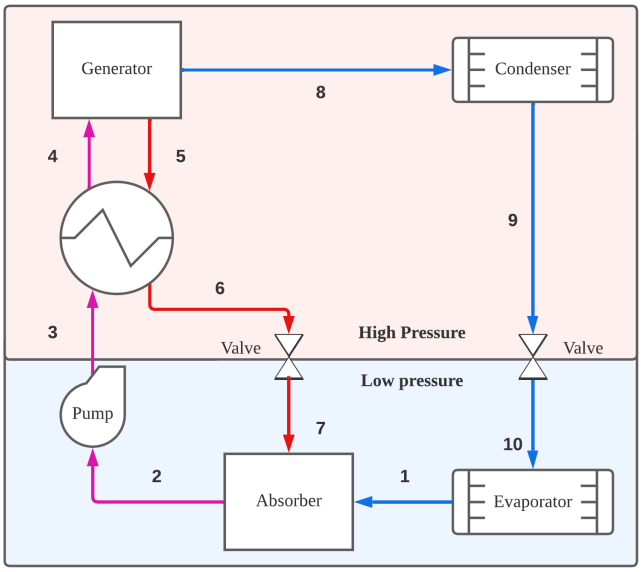


Figure. 1: Schematic representation of a basic absorption refrigeration cycle. The crimson-shaded area represents the high-pressure zone, while the blue area is the low-pressure zone. Additionally, the blue lines represent the refrigerant-rich flow, the crimson lines are the concentrated absorbent, and the violet lines concern the mixture between the refrigerant and the absorber.

$$f = \frac{\dot{m}_2}{\dot{m}_1} = 1 + \frac{\dot{m}_7}{\dot{m}_1} \tag{1}$$

where $\dot{m}_2$ is the mixture with the absorbed refrigerant, $\dot{m}_1$ is the refrigerant-rich flow from the evaporator, and $\dot{m}_7$ is the quasi-pure absorbent flow. A mass balance yields a simpler expression for the flow ratio. Also, applying the pure thermodynamic equilibrium criteria, Eq. (1) can be re-written as

$$f = \frac{x_{r,1} - x_{r,7}}{x_{r,2} - x_{r,7}} \tag{2}$$

where the subscript r concerns the refrigerant-rich flows.

The flow ratio is always a positive value commanded by the capability of the absorber to capture the refrigerant. In contrast, slight variations in the thermodynamic equilibrium at the absorber and generator pressure can yield feasibility problems in an accurately modelled cycle. In the latter case, an optimisation is required, particularly in the pressure of the generator and condenser. Despite this fact, the generator temperature can be manipulated, yielding a change in the conditions of the condenser. It is important to note that in the case of an ideal absorption cycle modelling, the flow ratio is reduced to $f \approx 1/x_{r,2}$. Therefore, an ideal absorption refrigerator cycle cannot present mass balance issues which, however, may emerge in many refrigerant/absorbent mixtures when a non-ideal behaviour of the cycle is considered.

The energy balances of the system are straightforward. In this framework, each enthalpy is defined by three parameters; temperature, volume, and mole fractions, i.e. $\tilde{H}_i = \tilde{H}_i\,(T_i,\ \tilde{v}_i,\ x_i)$. The general energy balance is reads

$$Q_g + Q_e + W_p = Q_c + Q_a \tag{3}$$

where the subscripts g, e, p, c, and a refer to the generator, evaporator, pump, condenser, and absorber, respectively.

On the one hand, the mechanical work of the pump is given by an isochoric compression with a mechanical efficiency of $\eta_p = 1.00$, which yields

$$\frac{W_p}{\dot{m}_1} = \frac{f}{\eta_p}\tilde{v}_2\,(P_3 - P_2) = \frac{f}{\eta_p}(\tilde{H}_3 - \tilde{H}_2) \tag{4}$$

On the other hand, the heat required by the generator can be calculated as

$$\frac{Q_g}{\dot{m}_1} = \tilde{H}_8 - \tilde{H}_6 + f\left(\tilde{H}_6 - \tilde{H}_3\right) \tag{5}$$

Consequently, the absorbed heat at the evaporator is simply given by

$$\frac{Q_e}{\dot{m}_1} = \tilde{H}_1 - \tilde{H}_{10} \tag{6}$$

Finally, the coefficient of performance (COP) of the cycle is given by

$$\mathrm{COP} = \frac{\tilde{H}_1 - \tilde{H}_{10}}{\tilde{H}_8 - \tilde{H}_6 + f\left(\tilde{H}_6 - \tilde{H}_3 + \frac{\tilde{H}_3 - \tilde{H}_2}{\eta_p}\right)} \tag{7}$$

The base configuration for analysing the cycle is taken from Yokozeki [24], where different temperatures for each piece of equipment are fixed. The generator operates at 373.15 K, while the condenser has a temperature of 313.15 K. The absorber is considered to be at thermodynamic equilibrium at 303.15 K, while the evaporator lies at 283.15 K. The aforementioned values are typical operational parameters for an absorption refrigeration cycle. Consequently, it can be assumed that the pressures will depend on the liquid-vapour equilibrium of the chosen refrigerant.

Additionally, ASHRAE explicitly states that the design pressure should not be less than the pressure arising under maximum operating, standby, or shipping conditions; in this case, the atmospheric pressure [64]. This condition can be considered a technical requirement to pre-screen the feasibility of the original list of refrigerants: they must exhibit a vapour pressure higher than the atmospheric one at the evaporator temperature (283.15 K). This restriction immediately excludes seven refrigerants from the analysis. The details of the technical criteria for each refrigerant, as well as the vapour pressures of the refrigerants at the evaporator and condenser temperatures, are shown in Table 1.

2.2. Working fluids modelling

SAFT and its different versions represent a family of molecular-based equations of state [66–68] rooted on statistical mechanics principles [69–71]. These models are capable of rendering the phase behaviour and thermophysical properties of a wide variety of compounds, including associating and highly polar species [72–74]. One of the most popular embodiments of these models is the PC-SAFT EOS [75, 76], a highly reputed version given its proven versatility and accuracy in representing real substance behaviour. The working fluids used in this work had already been successfully modelled with this approach [6, 11, 77, 78].

SAFT-type EOSs are expressed as a sum of contributions to the residual Helmholtz energy function of a specific compound, $\tilde{A}^{\mathrm{r}}$. In the particular structure of PC-SAFT, the contributions to the Helmholtz energy function concern the addition of different physical characteristics of the molecule, such as the hard chain, dispersive forces, and physical association. For the case of a non-polar compound, the equation reads

$$\tilde{A}^{\mathrm{r}} = \tilde{A}^{\mathrm{hc}} + \tilde{A}^{\mathrm{disp}} + \tilde{A}^{\mathrm{a}} \tag{8}$$

The superscripts in Eq. (8) concern hard-chain, dispersive, and association contributions, respectively. Further details of the EOS model can be found in the original work [75].

The total Helmholtz energy is completed by adding the ideal contribution, i.e. $\tilde{A} = \tilde{A}^{\mathrm{r}} + \tilde{A}^{\mathrm{i}}$, where $\tilde{A}^{\mathrm{i}}$ is given by

$$\frac{\tilde{A}^{\mathrm{i}}}{RT} = -\ln\tilde{v} - \frac{1}{RT}\iint\frac{C_P^{\mathrm{i}} - R}{T}dT^2 + \ln\frac{RT^{\Theta}}{P^{\Theta}} + \tilde{A}^{\mathrm{i}\Theta} \tag{9}$$

In Eq. (9), T^{Θ}, P^{Θ} and $\tilde{A}^{\mathrm{i}\Theta}$ are the temperature, pressure and perfect gas Helmholtz energy of a reference state, Θ, respectively. Additionally, C_P^{i} is the isobaric heat capacity of the perfect gas, which can be expressed in a polynomial form as

$$\frac{C_P^{\mathrm{i}}}{R} = \alpha_0 + \alpha_1 T + \alpha_2 T^2 + \alpha_3 T^{-2} + \alpha_4 T^3 \tag{10}$$

where, R is the universal gas constant, and α_i are the parameters obtained from the polynomial correlation. While the thermal part of the ideal term is usually omitted in vapor-liquid equilibrium calculations, it has an impact on the evaluation of the enthalpy and entropy values, and is preserved in the presented formulation. Ideal gas isobaric heat capacities are readily accessible in the literature. For common refrigerants, these values have been sourced from the DIPPR database [79], while for compounds without available data, the information has been derived through parametrization using equilibrium data [6]. In the case of DES, the heat capacities have been determined based on molecular structure, employing the group contribution

Table 1: Comparison between the reference and the PC-SAFT predicted pressure for the evaporator and condenser along with the technical criteria: (1) Satisfies the technical criteria and (2) Do not satisfy the technical criteria.

Name	R-number	Evaporator pressure (bar)		AAD	Condenser pressure (bar)		AAD	Tech. crit.
		NIST*	PC-SAFT		NIST*	PC-SAFT		
Hydrocarbons								
Isobutane	R600a	2.2061	2.2143	0.3717	5.3121	5.3146	0.0471	(1)
Neopentane	-	1.0315	1.0348	0.3199	2.6987	2.6957	0.1112	(1)
Isopentane	R601a	0.5231	0.5247	0.3116	1.5151	1.5188	0.2442	(2)
Isohexane	-	0.1460	0.1453	0.4454	0.5071	0.5066	0.0927	(2)
Isoheptane	-	-	0.0460	-	-	0.1718	-	(2)
Cyclohexane	-	0.0634	0.0639	0.7775	0.2464	0.2462	0.0893	(2)
Hydrofluorocarbons								
1,1,1,2,3,3,3-heptafluoropropane	R227ea	2.7957	2.8132	0.6256	7.0245	7.0939	0.9888	(1)
1,1,1,3,3,3-hexafluoropropane	R236fa	1.5972	1.6374	2.5150	4.3672	4.4299	1.4349	(1)
1,1,1,2,3,3-hexafluoropropane	R236ea	1.1812	1.1848	0.3089	3.3743	3.3730	0.0385	(1)
1,1,1,3,3-pentafluoropropane	R245fa	0.8242	0.8400	1.9165	2.5065	2.5230	0.6601	(2)
1,1,2,2,3-pentafluoropropane	R245ca	0.5404	0.5642	4.4129	1.7330	1.7598	1.5465	(2)
1,1,1,2-tetrafluoroethane	R134a	4.1461	4.1417	0.1061	10.166	10.164	0.0157	(1)
Hydrofluoroolefins								
2,3,3,3-tetrafluoropropene	R1234yf	-	4.4451	-	-	10.333	-	(1)
3,3,3-trifluoropropene	R1243zf	-	3.7514	-	-	8.8412	-	(1)
1,3,3,3-tetrafluoropropene	R1234ze(E)	-	3.0839	-	-	7.6834	-	(1)
1-chloro-3,3,3-trifluoropropene	R1233zd	-	0.7186	-	-	2.1144	-	(2)

*The column 'NIST' correspond to the models available is NIST's web page of Thermophysical Properties of Fluid Systems

The specific references for the technical EOS are not cited in this work. However, most of then are compiled in the work of Span [65]

Table 2: Parameters of Eq. (10) for the isobaric heat capacity of hydrocarbons, hydrofluorocarbons, hydrofluoroolefins and DESs tested in absorption refrigeration cycles.

R-number or shortcut	α_0	α_1 $\cdot 10^2$	α_2 $\cdot 10^5$	α_3	α_4 $\cdot 10^8$	T. range K	Source
R600a	2.7742	3.5937	–1.1060	–43767.70	0.0000	200.00-1500.00	[79]
Neopentane	3.5379	4.4652	–1.2188	–93539.26	0.0000	200.00-1500.00	[79]
R227ea	11.4525	2.9941	–1.4029	–250545.45	0.0000	200.00-1500.00	[79]
R236fa	28.5248	–4.4111	4.7924	–423569.64	0.0000	223.15-367.85	[6]
R236ea	9.0321	3.1804	–1.4660	–199252.44	0.0000	223.15-367.85	[6]
R134a	0.1156	4.4116	–3.8776	0.00	1.2857	273.00-1000.00	-
R1234yf	–2.9847	7.1498	–8.1282	15699.73	0.0000	223.15-367.85	[6]
R1243zf	–3.0828	7.3849	–8.3955	16215.99	0.0000	250.00-370.00	[6]
R1234ze-E	–3.1271	7.4909	–8.5159	16448.70	0.0000	183.15-382.55	[6]
[ChCl][EG][1]	2.8046	3.8526	–1.1562	0.00	–0.1936	273.00-1000.00	-
[ChCl][LA][2]	3.3418	5.4163	–1.9211	0.00	–0.1309	273.00-1000.00	-
[ChCl][Ph][3]	–2.9157	7.4383	–5.2560	0.00	1.5034	273.00-1000.00	-
[C2mim][H][4]	–8.6409	14.1013	–15.9271	0.00	7.2810	273.00-1000.00	-

1: [ChCl]+Ethylene Glycol (1:2), 2: [ChCl]+Levulinic Acid (1:2), 3: [ChCl]+Phenol (1:2). 4: $[C_2mim][Cl]+HC_4F_9CO_2$ (1:1).

Table 3: PC-SAFT molecular parameters of hydrocarbons, hydrofluorocarbons, hydrofluoroolefins and DESs.

Compound	m	σ	ε/k_B	$\sigma^{\Omega\Psi}$	$\varepsilon^{\Omega\Psi}/k_B$	AARD	Ref.
			Å	K	Å	K	$\tilde{v}^L$
R600a	2.2012	3.7933	219.71	0.00000	0.00	0.38	[6]
Neopentane	2.3543	3.9550	225.69	0.00000	0.00	1.59	[75]
R227ea	3.6601	3.2621	161.06	0.00000	0.00	0.78	[75]
R236fa	3.6592	3.2500	171.13	0.00000	0.00	1.70	[20]
R236ea	3.6356	3.1844	178.70	0.00000	0.00	1.70	[20]
R134a	3.2483	3.0157	170.60	0.00000	0.00	0.07	[81]
R1234yf	2.8978	3.3648	174.91	0.00000	0.00	1.70	[20]
R1243zf	2.7112	3.3960	186.08	0.00000	0.00	0.75	[82]
R1234ze(E)	3.2268	3.1909	173.87	0.00000	0.00	0.60	[82]
[ChCl][EG]	3.5808	3.2782	465.07	0.00211	4971.99	0.15	[72]
[ChCl][LA]	3.4672	3.6847	477.72	0.00300	4601.31	0.15	[72]
[ChCl][Ph]	2.6552	3.8998	490.63	0.00136	5208.99	0.15	[72]
[C_2mim][H]	4.4160	3.6400	336.20	0.00225	3450.00	0.01	-

method proposed by Joback et al. [80] and applied by Haghbakhsh et al. [60]. All constants are summarised in Table 2.

In this work, all refrigerants have been modelled as non-associating compounds, while the absorbents are treated as pseudo-fluids with a 2B association scheme. This scheme has been tested with good results in predicting the properties of DESs with different SAFT models [72, 83–85]. The molecular parameters of the refrigerants, which passed the primary test for the systems, and the 4 DESs, are listed in Table 3 [6, 75, 82].

The evaluation of the refrigerant-absorbent mixtures can be typically done through the use of binary interaction parameters to better adjust their solubility behaviour. However, it was decided to set all parameters to zero, due to the absence of experimental data. Although this may potentially affect the accuracy of the predictions, the flow concentrations typically fall within a range where an additional fit has minimal influence, provided that the system contains almost pure refrigerant or a low refrigerant concentration in the DES. Consequently, a well-parameterised pure compound has a strong capability to predict these systems, even when the interaction parameter is set to zero. As an additional test, the density of the [C_2mimCl][$HC_4F_9CO_2$] plus R134a mixture is satisfactorily rendered with a zero interaction parameter in the dispersive energy [86].

3. Evaluation and feasibility

On the one hand, three groups of refrigerants have been chosen based on their popularity. The first group are hydrocarbons (HCs), which have negligible GWP, but present other handicaps, such as their elevated flammability. The second group are third-generation hydrofluorocarbons (HFCs), currently prevalent in many uses, particularly in refrigeration. The last group is composed of fourth-generation hydrofluoroolefins (HFOs), characterised by its low GWP and almost isentropic behaviour [6], but with moderate flammability. On the other hand, four DES have been selected for analysis: [ChCl][Cl] + ethylene glycol, [ChCl][Cl] + lactic acid, and [ChCl][Cl] + phenol are different standard low-cost and environmentally friendly DESs with varying types of hydrogen bond donors. The last DES is an ionic liquid-based DES with proven performance in refrigerant absorption, as a result of its fluorinated anion [86]. As mentioned before, seven refrigerants have been immediately discarded by the technical criteria presented in Table 1, i.e. the range of pressure and temperature are unsuitable in the present case.

One additional requirement to consider concerns the feasibility of the absorber unit, which is restricted by the thermodynamic phase behaviour at the two considered pressures of the system. As an example, Fig. 2 shows the details of two isobars of a test system. The quasi-pure refrigerant at point (1) is combined with the mixture coming from the generator, whose concentration is fixed by the equilibrium at the generator pressure, highlighted in points (5), (6), and (7). Therefore, the mass balance in the absorber can not be fulfilled, as seen in point (2), making the equilibrium at the absorber unattainable. Although the problem caused by the phase equilibrium at the selected pressures can be avoided by modifying the pressure, particularly in the generator, this modification can result in a severe efficiency loss, making the working fluid technically inefficient. Alternatively, the cycle layout can be modified to enrich flow (7), for example, rectifying flow (5). The negative mass flow at the imposed conditions is considered a third criterion to establish the suitability of the refrigerant/absorbent combination. It is important to remind that this may only occur when considering a rigorous mass balance (if a pure-refrigerant flow is considered in the evaporator, the flow ratio is always positive). In summary, all working pairs exhibiting a negative flow ratio from the solubility calculation at specified pressures

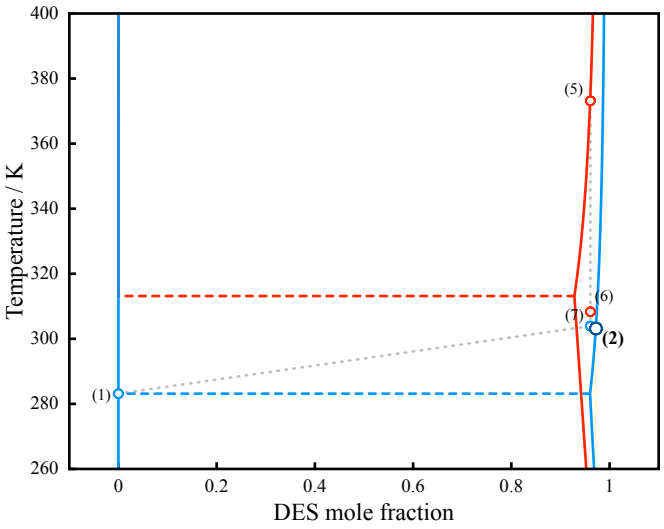


Figure. 2: Example of the phase behaviour at two pressures for a test system displaying an impossible combination of mass flow at the absorber.

are unsuitable for absorption cycles and must be removed from the analysis.

The combination of [ChCl]:Phenol (1:2) and R1234yf is selected as an example to facilitate an understanding of the absorption cycle, as this mixture is one of the suitable combinations accomplishing all previous criteria. Figures 3(a)-3(f) show the cycle represented in the concentration *vs.* temperature, density *vs.* temperature, and enthalpy *vs.* temperature. Open circles represent the mass flows listed in Fig. 1, dashed lines correspond to three-phase equilibrium, and dotted lines indicate the limit of the pure DES in Figs. 3(c)-3(f). All the projections are plotted at constant pressure, where isobars in blue represent the low pressure of the cycle (4.44 bar in this example), and isobars in crimson refer to the high operating pressure (10.33 bar). All calculations have been performed under several assumptions: 1-pressure drop in all equipment is neglected; 2-mass transfer effects are not considered; and 3- The pump and expansion valve are considered perfectly isentropic and isenthalpic, respectively.

The most intuitive projection is the concentration *vs.* temperature shown in Fig. 3(a)-(b), showing the phase, temperature, and composition of each flow. It is noted that the quasi-pure refrigerant flows are at approximately $x_1 = 0$. In contrast, the flow of the absorber part of the cycle lies over the equilibrium with a significant concentration of DES. The pressure lies in a narrow range of temperature. For this reason, a detail of the operating pressure range is shown in Fig. 4. In this mixture, points (1), (10), and (9) are slightly above the three-phase line. However, the amount of DES presented in these flows is insignificant. Moreover, flow (8) is at a higher temperature caused by the generator process. Flows (3) and (6) are subcooled homogeneous fluids. The first is caused by the isentropic compression of a saturated liquid mixture, while the second is produced by an isobaric quenching at the heat exchanger. Points (2), (4), and (5) are DES-rich saturated liquids. Additionally, point (7) comes from an isenthalpic flow expansion (6); hence, it is a liquid-vapour equilibrium state with a small vaporised fraction.

Figures 3(c)-(d) show the density of each mass flow. The phase difference in the quasi-pure refrigerant can be clearly distinguished in this projection. For instance, points (8)-(9) and (10)-(1) have a dramatic change in their density. From (10) to (1), the absorption heat in the evaporator yields the disappearance of the liquid phase. At the same time, the isenthalpic expansion causes a slight reduction in the density, almost imperceptible on the graph. Flow (8) lies at a higher temperature for the same reason previously raised. An additional interesting feature is an isopycnic point between the two liquid phases at low temperatures. This isopycnic point is also barotropic and can be glimpsed in all the DES-refrigerant studied mixtures [87, 88]. However, this behaviour does not interfere with the system at the studied conditions.

Finally, the temperature *vs.* enthalpy representation measures the change in energy, mainly in the evaporator and condenser. It is important to note that there is a temperature drop from points (8) to (9), caused by the transition between the generator and the condenser. As a consequence, condensation of the refrigerant-rich liquid phase is observed. The refrigerant flow is expanded to point (10) in the valve.

On the one hand, the performance of the cycle is directly related to the position of the two liquid phases formed in the mixture because it limits the evaporator heat. On the other hand, the generator-required heat is sensitive to pressure and to the heat source, being driven by the liquid-vapour equilibrium of the system. For this reason, the COP of this kind of system is restricted to low values.

Among the 64 original mixtures, 28 have not passed the basic criteria to be applied in an absorption refrigeration cycle, i.e. to be over the atmospheric pressure at the evaporator temperature. From the remaining 36, half of the candidates have been discarded by the thermodynamic criteria, yielding a negative flow ratio in the analysed conditions. Finally, 18 mixtures are suitable to be used in the system. However, the calculation of the COP reveals important differences in these systems.

Table 4 summarises all the combinations of refrigerants and absorbents classified according to the imposed criteria. In this table, the grey mixtures correspond to the omitted systems due to their technical condition. The crimson mixtures have thermodynamic impediments (negative flow), while the green mixtures are suitable to be used in ARCs. Besides, the different shades of green represent the magnitude of the COP of the system, from the lower in the case of [ChCl][EG] + R236ea (a very subtle shade of green almost white) to the higher performed mixture composed by [C_2mim][H] + R227ea.

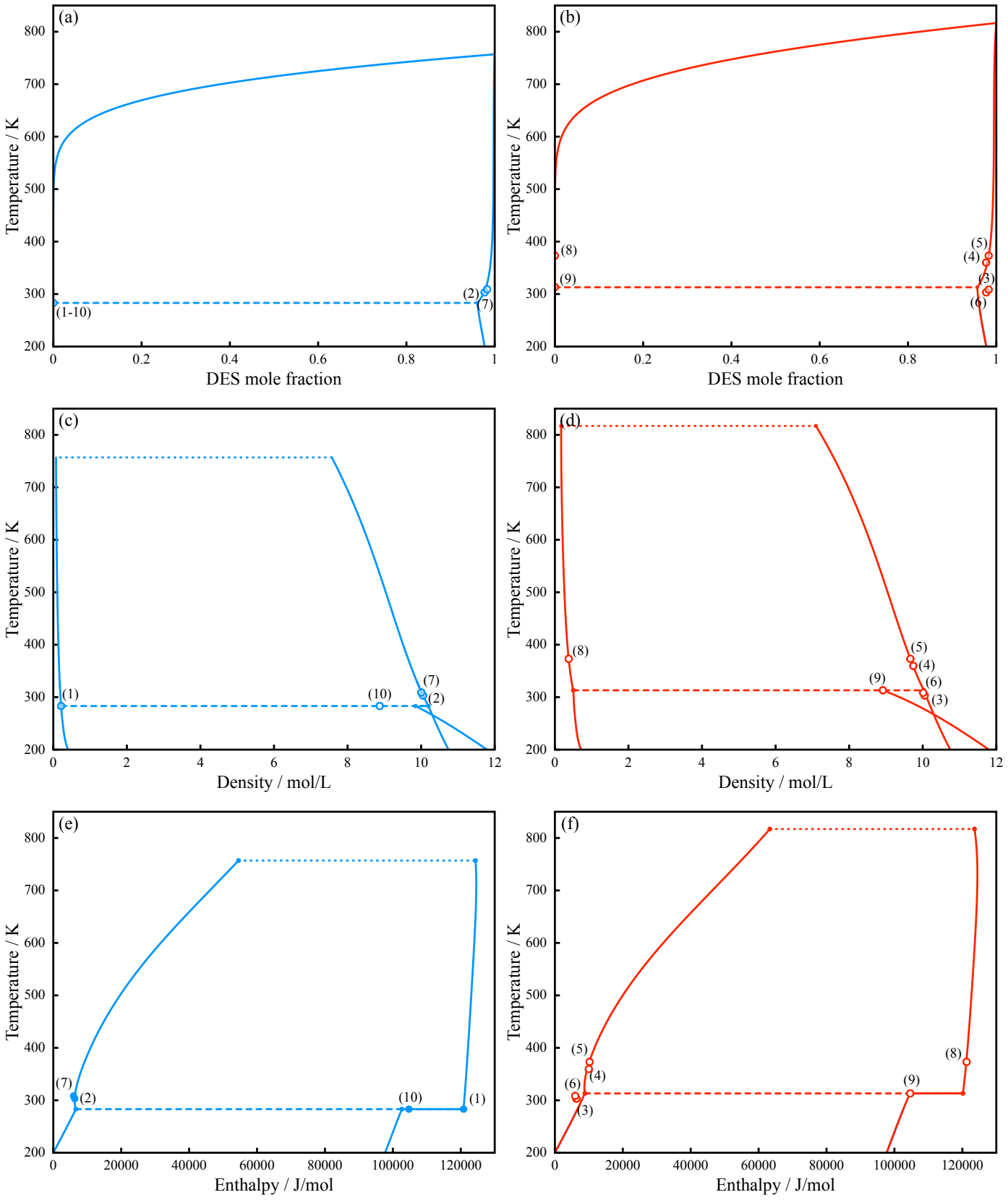


Figure. 3: Projections of an absorption cycle operating with [ChCl][Phenol] (1:2) plus R1234yf. (a)-(b) temperature *vs.* concentration, (c)-(d) temperature *vs.* density, and (e)-(f) temperature *vs.* enthalpy at 4.44 bar in blue and 10.33 bar in crimson.

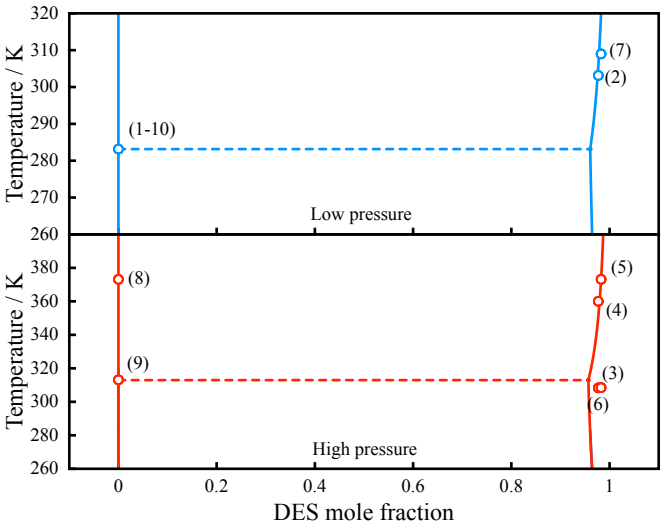


Figure. 4: Detail of Figs. 3(a) and 3(b) showing the concentration *vs.* temperature diagrams for the [ChCl][Phenol] (1:2) plus R1234yf system.

Table 4: General view of the analysed working mixtures and its application in ARCs. Grey indicates technically inadequate mixtures, crimson stands for thermodynamically unfeasible systems, while shades of green highlight the suitable mixtures. Green intensity is related to the COP value.

	[ChCl][EG]	[ChCl][LA]	[ChCl][Ph]	[C2mim][H]
Isobutane				
Neopentane				
Isopentane				
Isohexane				
Isoheptane				
Cyclohexane				
R227ea				
R236fa				
R236ea				
R245fa				
R245ca				
R134a				
R1233zd				
R1234yf				
R1234ze				
R1243zf				

Table 5: Values of COP, CR, GWP, and ASHRAE classification for the 18 suitable working mixtures in a DES-based absorption cycle.

Mixture	COP	CR	GWP	Class
R600a + [C2mim][H]	0.32	2.4001	3.3	A3
Np + [C2mim][H]	0.11	2.4050	3.0	-
R134a + [C2mim][H]	0.63	2.4542	1300	A1
R227ea + [ChCl][LA]	0.72	2.5216	3350	A1
R227ea + [ChCl][Ph]	0.27	2.5217	3350	A1
R227ea + [C2mim][H]	0.92	2.5217	3350	A1
R236ea + [ChCl][EG]	0.02	2.8467	1370	A2
R236ea + [ChCl][LA]	0.64	2.8468	1370	A2
R236ea + [ChCl][Ph]	0.69	2.8469	1370	A2
R236ea + [C2mim][H]	0.74	2.8469	1370	A2
R236fa + [ChCl][Ph]	0.51	2.7054	8060	A1
R236fa + [C2mim][H]	0.49	2.7054	8060	A1
R1234yf + [ChCl][Ph]	0.22	2.3245	<1	A2L
R1234yf + [C2mim][H]	0.30	2.3245	<1	A2L
R1234ze + [ChCl][Ph]	0.52	2.4915	<1	A2L
R1234ze + [C2mim][H]	0.59	2.4915	<1	A2L
R1243zf + [ChCl][Ph]	0.31	2.3568	<1	A2
R1243zf + [C2mim][H]	0.41	2.3568	<1	A2

Obviously, the choice of the best working fluid pair cannot be done by exclusively analysing its technical efficiency (COP). Additional safety and environmental requirements, such as toxicity, GWP, and flammability must be considered when selecting an adequate working mixture.

Table 5 presents the raw values of the COP, GWP, flammability (FLM), and compression ratio (CR) for a more global analysis. In order to complete the flammability classification, the value of R236ea has been assigned to the A2 class. A similar case can be seen for neopentane, which has been homologated to other hydrocarbons.

From these results, it can be noticed the necessity to rigorously consider the non-ideal separation of the pair absorbent-refrigerant, unravelling many unfeasible systems. To our knowledge, this is reported for the first time, as those systems are commonly modelled assuming ideal behaviour of the separation in the generator. It is remarkable that [ChCl][EG] is an unsuitable absorbent for all refrigerants, including hydrocarbons and fluorinated gases, except for R236ea, where the COP is negligible. Interestingly, the IL-based DES presents the most promising properties for absorption, becoming suitable in all cases, and offering the best performance in combination with R227ea. Hydrocarbons can only be used with the IL-based DES, while R227ea and R236ea are the refrigerants with better properties for most of the selected DES. Concerning hydrofluoroolefins, these fourth-generation refrigerants work with both [ChCl][Ph] and [C_2mim][H], but provide low COP values.

Finally, the four Key Perfomance Indicators (KPIs), the

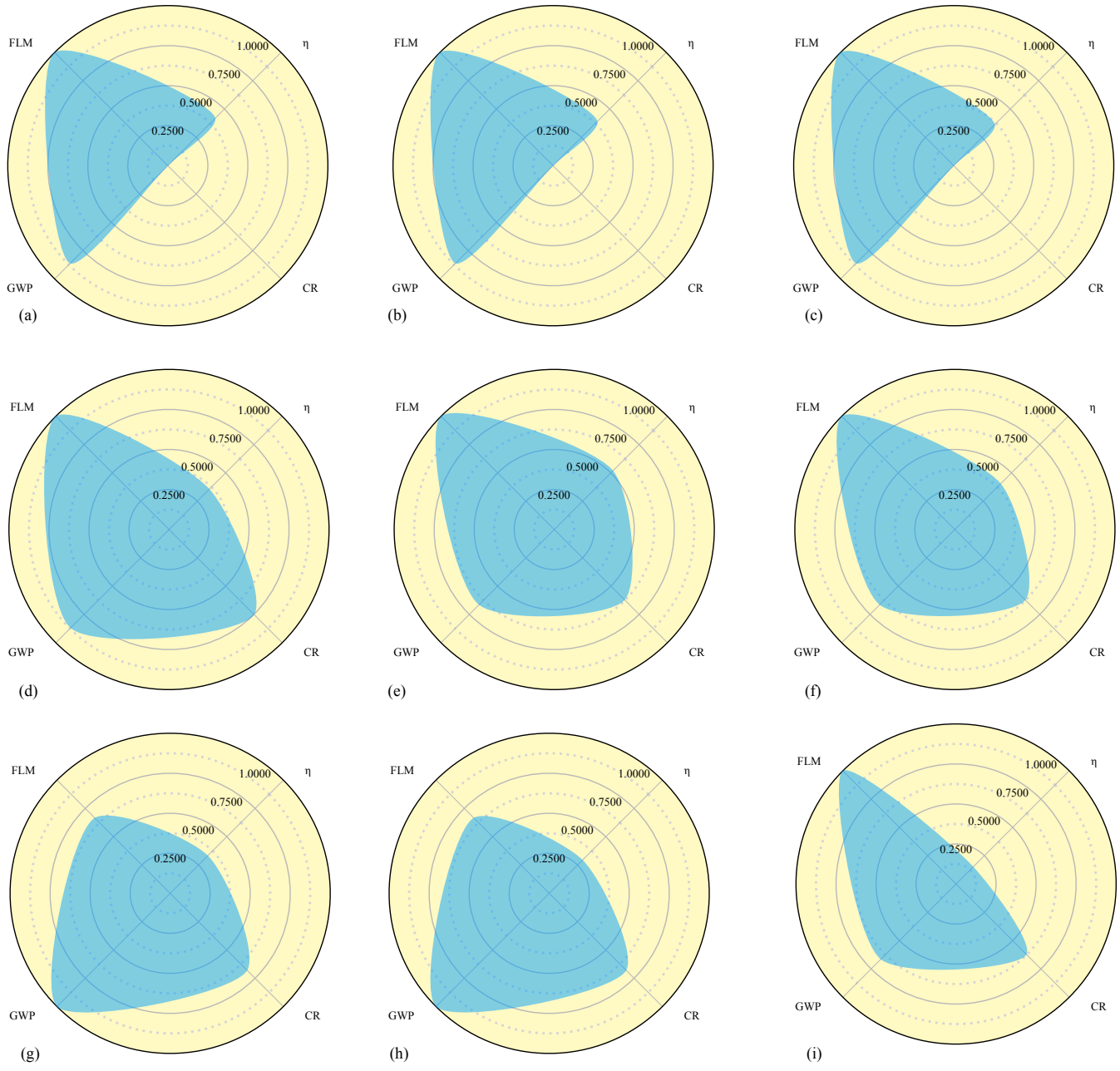


Figure. 5: Radar plots of the capability of the best nine working mixtures in a DES-based absoption cycle. a) R236ea + [C_2mim][H], b) R236ea + [ChCl][Ph], c) R236ea + [ChCl][LA], d) R134a + [C_2mim][H], e) R227ea + [C_2mim][H], f) R227ea + [ChCl][LA], g) R1234ze + [C_2mim][H], h) R1234ze + [ChCl][Ph], and i) R227ea+[ChCl][Ph].

COP, GWP, FLM, and CR are compared in radar plots to build a holistic examination of the mixtures. To a better understanding, the variables are normalised to reach their larger values when they become beneficial to the system, i.e. less flammability and less toxicity mean higher values in the axis. The COP is presented as the normalised efficiency as $\eta = \mathrm{COP}/\mathrm{COP_C}$, where $\mathrm{COP_C}$ is the COP of an equivalent Carnot refrigeration cycle. The GWP is normalised using a linear regression between 1 to 10000 units, and the flammability by discretising between zero to one the flammability categories "1", "2", "2L", and "3". Finally, the CR, P_3/P_2, is presented between zero and one, where zero is the larger value (2.85) and one the minor value (2.32), denoting the energy consumption of the pump.

Figure 5 shows the radar plots of the nine better working mixtures among the eighteen suitable combinations (the rest of them can be found in the Supplementary Material of the manuscript). Overall, the best performances correspond to the working pairs with highest blue area. The most attractive working mixtures are always composed of [C_2mim][H] or [ChCl][Ph] as absorbent and R236ea or R227ea as the refrigerant. It is important to note that if the compression necessities are considered, the use of HFOs becomes more attractive. However, the low energy consumption of the liquid compression, compared to the energy required in the generator, suggests that this parameter is not comparable with others and should have a minor weight.

4. Concluding remarks

This work has been devoted to modelling an absorption refrigeration cycle composed of a standard layout, including a heat exchanger between the absorber and the generator. Three Choline Chloride-based and one IL-based DESs have been used as absorbers, while sixteen fluids have been selected as refrigerants. The latter includes hydrocarbons and a set of third and fourth generation fluorinated refrigerants. The PC-SAFT model has been used to evaluate the thermophysical properties of these compounds at the operating conditions of the cycle.

The accurate modelling of an absorption cycle highlights that the phase behaviour of the working mixture at high DES concentration limits the range of temperature and pressure of operation of the cycle. For that reason, optimising procedures are needed in many cases. In addition, it has been demonstrated that the ideal modelling of the absorption cycle is unsuitable for rendering the actual capabilities and restrictions of these systems, especially with complex working mixtures.

From the original sixty-four possible combinations, only eighteen were suitable for ARCs, passing the technical and thermodynamic criteria. However, the efficiency of most mixtures in terms of COP remains modest. The IL-based DES is the most promising absorbent for this kind of cycle using fluorinated gases, while R227ea and R236ea have good capability to be absorbed in DESs. A whole analysis adding information on the GWP, flammability, toxicity, and compression ratio yield similar results, with the R227ea + [C_2mim][H] exhibiting the best performance.

Acknowledgement

C. Imas acknowledges the support of *Magister en Ingeniería Mecánica* (MIM) of Universidad de Talca and funding from FONDECYT, Chile (project no. 11180103), H.Q.-L. acknowledges funding from FONDECYT, Chile (project no. 11180103) and J.M.G. acknowledges funding from FONDECYT, Chile (project no. 1230236) and FOVI220054. Additional funding support from the Spanish Ministry of Science and Innovation MCIN/AEI/10.13039/501100011033 and by the European Union NextGenerationEU/ PRTR under R+D+I projects STOP-F-Gas (Ref: PID2019-108014RB-C21) and NEW-F-Tech (Ref: TED2021-130959B-I00) is gratefully acknowledged.

Supplementary material

The Supplementary material includes the raw and normalised data for all the analysed working mixtures and the radar plots of the combinations not presented in the main body of the work.

List of symbols

$\tilde{A}_i$: Helmholtz energy function at point i. C_P^{i}: Isobaric heat capacity of the perfect gas. f: flow ratio defined in Eq. (1). $\tilde{H}_i$: enthalpy at point i. m: segment number parameter of PC-SAFT. P_i: pressure at point i. Q: Heat of the isobaric processes. R: Universal gas constant. T_i: thermodynamic temperature at point i. $\tilde{v}_i$: molar volume at point i. W: Thermodynamic work.

Subscripts and superscripts

g: refers the generator. e: refers the evaporator. p: refers the pump. c: refers the condenser. a: refers the absorber. r: refers the residual contribution of the EOS. hc: refers the hard-chain contribution of the EOS. disp: refers the dispersive contribution of the EOS. a: refers the association contribution of the EOS.

Greek letters

α_i: Parameter of the polynomial heat capacity defined in Eq. (10). ε/k_B: energy parameter of PC-SAFT. $\varepsilon^{\Omega_i\Psi_i}/k_B$: Association volume. η_p: isentropic efficiency. Θ: refers the reference state of the Helmholtz energy function. $\sigma^{\Omega_i\Psi_i}$: Association volume. σ: segment diameter parameter of PC-SAFT.

Abbreviations

ARC: Absorption refrigeration cycle. **ASHRAE:** American Society of Heating, Refrigerating and Air-Conditioning Engineers. **ChCl:** Choline Chloride. **COP:** Coefficient of performance. **COSMO-RS:** Conductor like screening model for real solvents. **DES:** Deep eutectic solvent. **EOS:** Equation of state. **F-gas:** Fluorinated gas. **GHG:** Greenhouse gas. **GWP:** Global Warming Potential. **HBA:** Hydrogen bond acceptor. **HBD:** Hydrogen bond donor. **HFC:** Hydrofluorocarbon. **HFO:** Hydrofluoroolefin. **ODP:** Ozone depletion potential. **PC-SAFT:** Perturbed-chain Statistical association fluid theory. **ORC:** Organic Rankine cycle. **VCR:** Vapour compression refrigeration.

Author information

Corresponding author

Héctor Quinteros-Lama – Departamento de Tecnologías Industriales, Faculty of Engineering, Universidad de Talca. Merced 437, Curicó, Chile ORCID: 0000-0001-8953-6140; E-mail: hquinteros@me.com

References

[1] O. B. Adekoya, J. K. Olabode, S. K. Rafi, Renewable energy consumption, carbon emissions and human development: Empirical comparison of the trajectories of world regions, Renewable Energy 179 (2021) 1836–1848. doi:10.1016/j.renene.2021.08.019.

[2] V. Marchal, R. Dellink, Chapter 3, in: OECD Environmental outlook to 2050, 2011.

[3] United Nations: Climate Change, COP26 Explained, UN Chimate Change Conference UK 2021, 2021.

[4] T. Auld, M. P. McHenry, J. Whale, US military, airspace, and meteorological radar system impacts from utility class wind turbines: Implications for renewable energy targets and the wind industry, Renewable Energy 55 (2013) 24–30. doi:10.1016/j.renene.2012.12.008.

[5] V. Echarri-Iribarren, C. Rizo-Maestre, F. Echarri-Iribarren, Healthy climate and energy savings: Using thermal ceramic panels and solar thermal panels in Mediterranean housing blocks, Energies 11 (2018). doi:10.3390/en11102707.

[6] J. González, F. Llovell, J. M. Garrido, H. Quinteros-Lama, A rigorous approach for characterising the limiting optimal efficiency of working fluids in organic Rankine cycles, Energy 254 (2022) 124191. doi:10.1016/j.energy.2022.124191.

[7] M. Izanloo, Y. Noorollahi, A. Aslani, Future energy planning to maximize renewable energy share for the south Caspian Sea climate, Renewable Energy 175 (2021) 660–675. doi:10.1016/j.renene.2021.05.008.

[8] M. Molina, F. Rowland, Stratospheric sink for chlorofluoromethanes: chlorine atom-catalysed destruction of ozone, Nature 249 (1974) 810–812. doi:https://doi.org/10.1038/249810a0.

[9] A. Engel, M. Rugby, Chapter 2, in: Scientific Assessment of Ozone Depletion: 2018, World Meteorological Organisation Global Ozone Research and Monitoring Project-Report No. 58, 2018.

[10] A. Goyal, A. F. Sherwani, D. Tiwari, Optimization of cyclic parameters for ORC system using response surface methodology (RSM), Energy Sources, Part A: Recovery, Utilization, and Environmental Effects 43 (8) (2021) 993–1006. doi:10.1080/15567036.2019.1633443.

[11] J. Albornoz, A. Mejía, H. Quinteros-Lama, J. M. Garrido, A rigorous and accurate approach for predicting the wet-to-dry transition for working mixtures in organic Rankine cycles, Energy 156 (2018) 509 – 519. doi:10.1016/j.energy.2018.05.074.

[12] J. H. Kumar, A. Adisa, Life cycle environmental impacts of inhalers, Journal of Cleaner Production 237 (2019). doi:https://doi.org/10.1016/j.jclepro.2019.117733.

[13] T. Wen-Tien, An overview of environmental hazards and exposure risk of hydrofluorocarbons (HFCs), Chemosphere 61 (2005) 1539–1547. doi:https://doi.org/10.1016/j.chemosphere.2005.03.084.

[14] S. Andersen, P. Ashford, Safeguarding the Ozone Layer and the Global Climate System: Issues Related to Hydrofluorocarbons and Perfluorocarbons, IPCC/TEAP Special Report, 2002.

[15] Zero ODP HFC Blowing Agents for Appliance Foam, Journal of Cellular Plastics 33 (3) (1997) 207–218. doi:10.1177/0021955X9703300302.

[16] SKM Enviros, Phase Down of HFC Consumption in the EU - Assessment of Implications for the RAC Sector, 2012.

[17] M. O. McLinden, M. L. Huber, (r)evolution of refrigerants, Journal of Chemical & Engineering Data 65 (2020) 4176–4193. doi:10.1021/acs.jced.0c00338.

[18] H. Li, X. Bu, L. Wang, Z. Long, Y. Lian, Hydrocarbon working fluids for a Rankine cycle powered vapor compression refrigeration system using low-grade thermal energy, Energy and Buildings 65 (2013) 167–172. doi:10.1016/j.enbuild.2013.06.012.

[19] S. I. Ata, A. Kahraman, R. Sahin, Prediction and sensitivity analysis under different performance indices of R1234ze ORC with Taguchi s multi-objective optimization, Case Studies in Thermal Engineering 22 (2020) 100785. doi:10.1016/j.csite.2020.100785.

[20] G. Raabe, Molecular simulation studies on the vapor-liquid phase equilibria of binary mixtures of R-1234yf and R-1234ze(E) with R-32 and CO_2, Journal of Chemical & Engineering Data 58 (6) (2013) 1867–1873. doi:10.1021/je4002619.

[21] S. Gupta, N. K. Karanam, R. Konijeti, A. Dasore, Thermodynamic Analysis and Effects of Replacing HFC by Fourth-Generation Refrigerants in VCR Systems, International Journal of Air-Conditioning and Refrigeration 26 (2018) 02. doi:10.1142/S201013251850013X.

[22] Ashwni, A. F. Sherwani, D. Tiwari, Thermodynamic analysis of simple and modified organic Rankine cycle and vapor compression refrigeration (ORC-VCR) systems, Environmental Progress & Sustainable Energy 40 (3) (2021) 1–11. doi:10.1002/ep.13577.

[23] C. Yue, F. You, Y. Huang, Thermal and economic analysis of an energy system of an ORC coupled with vehicle air conditioning, International Journal of Refrigeration 64 (2016) 152–167. doi:10.1016/j.ijrefrig.2016.01.005.

[24] A. Yokozeki, Theoretical performances of various refrigerant–absorbent pairs in a vapor-absorption refrigeration cycle by the use of equations of state, Applied Energy 80 (1-6) (2005) 383399. doi:10.1016/j.apenergy.2004.04.011.

[25] L. Na, L. Chunhuan, S. Qingquan, A working pair of $CaCl_2$–LiBr–$LiNO_3$/H_2O and its application in a single-stage solar-driven absorption refrigeration cycle, International Journal of Refrigeration 86 (2018) 1–13. doi:https://doi.org/10.1016/j.ijrefrig.2017.11.004.

[26] M. Izquierdo, M. Venegas, P. Rodrıguez, A. Lecuona, Crystallization as a limit to develop solar air-cooled LiBr–H_2O absorption systems using low-grade heat, Solar Energy Materials and Solar Cells 81 (2004) 205–216. doi:https://doi.org/10.1016/j.solmat.2003.11.002.

[27] Z. Sai, H. Guogeng, L. Xiao, L. Yanfei, P. Qicong, C. Dehua, Experimental performance evaluation and comparison of an absorption refrigeration prototype driven by exhaust heat operating with NH_3/$LiNO_3$ and NH_3/$LiNO_3$+H_2O, International Journal of Refrigeration 132 (2021) 172–186. doi:https://doi.org/10.1016/j.ijrefrig.2021.09.015.

[28] T. M. Becker, M. Wang, A. Kabra, S. H. Jamali, M. Ramdin, D. Dubbeldam, C. A. Infante Ferreira, T. J. H. Vlugt, Ab-

sorption refrigeration cycles with ammonia–ionic liquid working pairs studied by molecular simulation, Industrial & Engineering Chemistry Research 57 (2018) 5442–5452. doi:10.1021/acs.iecr.8b00442.

[29] H. Valença de Araújo, L. H. Parolin Massuchetto, R. Barcelos Corrêa do Nascimento, S. M. Rocha de Carvalho, J. V. Hallak Dangelo, Thermodynamic performance analysis of a single-effect absorption refrigeration system operating with water and 1-ethyl-3-methylimidazolium-based ionic liquids mixtures, Applied Thermal Engineering 201 (2022) 117761. doi:10.1016/j.applthermaleng.2021.117761.

[30] L. Ding, L. Zijian, B. Yin, S. Shoujun, G. Maoqiong, S. Jun, Experimental study and economic analysis of an absorption refrigeration system with new generator structure applied for pre-cooling in liquefied natural gas plant, International Journal of Refrigeration 119 (2021) 78–87. doi:https://doi.org/10.1016/j.ijrefrig.2021.04.031.

[31] S. Pourhedayat, E. Hu, L. Chen, Simulation of innovative hybridizing M-cycle cooler and absorption-refrigeration for pre-cooling of gas turbine intake air: Including a case study for Siemens SGT-750 gas turbine, Energy 247 (2022) 123356. doi:10.1016/j.energy.2022.123356.

[32] N. Shokati, S. Khanahmadzadeh, The effect of different combinations of ammonia-water Rankine and absorption refrigeration cycles on the exergoeconomic performance of the cogeneration cycle, Applied Thermal Engineering 141 (2018) 1141–1160. doi:10.1016/j.applthermaleng.2018.06.052.

[33] Y. Ding, O. Olumayegun, Y. Chai, Y. Liu, M. Wang, Simulation, energy and exergy analysis of compressed air energy storage integrated with organic Rankine cycle and single effect absorption refrigeration for trigeneration application, Fuel 317 (2022) 123291. doi:10.1016/j.fuel.2022.123291.

[34] X. Lin, L. Zuo, L. Yin, W. Su, S. Ou, An idea to efficiently recover the waste heat of data centers by constructing an integrated system with carbon dioxide heat pump, mechanical subcooling cycle and lithium bromide-water absorption refrigeration cycle, Energy Conversion and Management 256 (2022) 115398. doi:10.1016/j.enconman.2022.115398.

[35] M. E. Álvarez, M. Bourouis, X. Esteve, Vaporliquid equilibrium of aqueous alkaline nitrate and nitrite solutions for absorption refrigeration cycles with high-temperature driving heat, Journal of Chemical & Engineering Data 56 (2011) 491–496. doi:10.1021/je1008894.

[36] R. Haghbakhsh, H. Peyrovedin, S. Raeissi, A. R. C. Duarte, A. Shariati, Investigating the performance of novel green solvents in absorption refrigeration cycles: Energy and exergy analyses, International Journal of Refrigeration 113 (2020) 174–186. doi:10.1016/j.ijrefrig.2020.01.013.

[37] R. Abedin, S. Heidarian, J. C. Flake, F. R. Hung, Computational evaluation of mixtures of hydrofluorocarbons and deep eutectic solvents for absorption refrigeration systems, Langmuir 33 (2017) 11611–11625. doi:10.1021/acs.langmuir.7b02003.

[38] Y. Gong, L. Yang, Z. Lu, L. Wang, H. Li, Thermodynamic performance assessment of ammonia/ionic liquid based half-effect absorption refrigeration cycle, Case Studies in Thermal Engineering 25 (2021) 100924. doi:10.1016/j.csite.2021.100924.

[39] M. Wang, T. M. Becker, B. A. Schouten, T. J. Vlugt, C. A. I. Ferreira, Ammonia/ionic liquid based double-effect vapor absorption refrigeration cycles driven by waste heat for cooling in fishing vessels, Energy Conversion and Management 174 (2018) 824–843. doi:10.1016/j.enconman.2018.08.060.

[40] Y. Sun, Y. Zhang, G. Di, X. Wang, J. M. Prausnitz, L. Jin, Vapor–liquid equilibria for R1234ze(E) and three imidazolium-based ionic liquids as working pairs in absorption–refrigeration cycle, Journal of Chemical & Engineering Data 63 (2018) 3053–3060. doi:10.1021/acs.jced.8b00314.

[41] S. Kim, N. Patel, P. A. Kohl, Performance simulation of ionic liquid and hydrofluorocarbon working fluids for an absorption refrigeration system, Industrial & Engineering Chemistry Research 52 (2013) 6329–6335. doi:10.1021/ie400261g.

[42] S. Kim, Y. J. Kim, Y. K. Joshi, A. G. Fedorov, P. A. Kohl, Absorption heat pump/refrigeration system utilizing ionic liquid and hydrofluorocarbon refrigerants, Journal of Electronic Packaging 134 (2012) 9. doi:10.1115/1.4007111.

[43] S. Kim, P. A. Kohl, Theoretical and experimental investigation of an absorption refrigeration system using R134/[bmim][PF_6] working fluid, Industrial & Engineering Chemistry Research 52 (2013) 13459–13465. doi:10.1021/ie400985c.

[44] A. P. Abbott, D. Boothby, G. Capper, D. L. Davies, R. K. Rasheed, Deep eutectic solvents formed between choline chloride and carboxylic acids: Versatile alternatives to ionic liquids, Journal of the American Chemical Society 126 (2004) 9142–9147. doi:10.1021/ja048266j.

[45] X. Duan, B. Gao, C. Zhang, D. Deng, Solubility and thermodynamic properties of NH_3 in choline chloride-based deep eutectic solvents, The Journal of Chemical Thermodynamics 133 (2019) 79–84. doi:10.1016/j.jct.2019.01.031.

[46] Y. Zhang, D. Poe, L. Heroux, H. Squire, B. W. Doherty, Z. Long, M. Dadmun, B. Gurkan, M. E. Tuckerman, E. J. Maginn, Liquid structure and transport properties of the deep eutectic solvent ethaline, J. Phys. Chem. B 124 (2020) 5251–5264. doi:https://doi.org/10.1021/acs.jpcb.0c04058.

[47] B. Gurkan, H. Squire, E. Pentzer, Metal-free deep eutectic solvents: Preparation, physical properties, and significance, J. Phys. Chem. Lett. 10 (2019) 7956–7964. doi:https://doi.org/10.1021/acs.jpclett.9b01980.

[48] L. S. Leonhardo, S. Pandey, S. Ravula, S. Pandey, Z. Hua, G. A. Baker, S. N. Baker, Ternary deep eutectic solvents tasked for carbon dioxide capture, ACS Sustainable Chem. Eng. 2 (2014) 2117–2123. doi:https://doi.org/10.1021/sc5001594.

[49] J. M. Silva, R. L. Reis, A. Paiva, A. R. C. Duarte, Design of functional therapeutic deep eutectic solvents based on choline chloride and ascorbic acid, ACS Sustainable Chem. Eng. 6 (2018) 10355–10363. doi:https://doi.org/10.1021/acssuschemeng.8b01687.

[50] A. Leal-Duaso, I. Favier, D. Pla, E. Pires, M. Gómez, Design of glycerol-based solvents for the immobilization of palladium nanocatalysts: A hydrogenation study, ACS Sustainable Chem. Eng. 9 (2021) 6875–6885. doi:https://doi.org/10.1021/acssuschemeng.1c01694.

[51] A. I. Akhmetshina, A. N. Petukhov, A. Mechergui, A. V. Vorotyntsev, A. V. Nyuchev, A. A. Moskvichev, I. V. Vorotyntsev, Evaluation of methanesulfonate-based deep eutectic solvent for ammonia sorption, Journal of Chemical & Engineering Data 63 (2018) 1896–1904. doi:10.1021/acs.jced.7b01004.

[52] G. García, M. Atilhan, S. Aparicio, Interfacial properties of deep eutectic solvents regarding to co2 capture, J. Phys. Chem. B 119 (2015) 21413–21425. doi:https://doi.org/10.1021/acs.jpcc.5b04585.

[53] A. Leal-Duaso, J. A. Mayoral, E. Pires, Steps forward toward the substitution of conventional solvents in the heck–mizoroki coupling reaction: Glycerol-derived ethers and deep eutectic solvents as reaction media, ACS Sustainable Chem. Eng. 8 (2020) 13076–13084. doi:https://doi.org/10.1021/acssuschemeng.0c04862.

[54] M. Cvjetko Bubalo, S. Vidović, I. Radojčić Redovniković, S. Jokić, Green solvents for green technologies, Journal of Chemical Technology & Biotechnology 90 (2015) 1631–1639. doi:10.1002/jctb.4668.

[55] E. Smith, A. Abbott, K. Ryder, Deep eutectic solvents (DESs) and their applications, Chemical Reviews 114 (2014) 11060–11082. doi:10.1021/cr300162p.

[56] L. I. N. Tomé, V. Baião, W. da Silva, C. M. A. Brett, Deep eutectic solvents for the production and application of new materials, Applied Materials Today 10 (2018) 30–50. doi:10.1016/j.apmt.2017.11.005.

[57] A. Paiva, R. Craveiro, I. Aroso, M. Martins, R. L. Reis, A. R. C. Duarte, Natural deep eutectic solvents – solvents for the 21st century, ACS Sustainable Chem. Eng. 2 (5) (2014) 1063–1071. doi:10.1021/sc500096j.

[58] R. Abedin, S. Heidarian, J. C. Flake, F. R. Hung, Computational evaluation of mixtures of hydrofluorocarbons and deep

eutectic solvents for absorption refrigeration systems, LANGMUIR 33 (2017). doi:10.1021/acs.langmuir.7b02003.
[59] R. Abedin, Y. Shen, J. C. Flake, F. R. Hung, Deep eutectic solvents mixed with fluorinated refrigerants for absorption refrigeration: A molecular simulation study, The Journal of Physical Chemistry B 124 (2020) 4536–4550. doi:10.1021/acs.jpcb.0c01860.
[60] R. Haghbakhsh, H. Peyrovedin, S. Raeissi, A. R. C. Duarte, A. Shariati, Energy conservation in absorption refrigeration cycles using DES as a new generation of green absorbents, Entropy 22 (2020) 1–19. doi:10.3390/e22040409.
[61] N. Wijeysundera, An irreversible-thermodynamic model for solar-powered absorption cooling systems, Solar Energy 68 (1) (2000) 69–75. doi:https://doi.org/10.1016/S0038-092X(99)00051-1.
[62] K. C. Ng, H. T. Chua, Q. Han, T. Kashiwagi, A. Akisawa, T. Tsurusawa, Thermodynamic modeling of absorption chiller and comparison with experiments, Heat Transfer Engineering 20 (2) (1999) 42–51. doi:10.1080/014576399271574.
[63] R. Romero, W. Rivera, R. Best, Comparison of the theoretical performance of a solar air conditioning system operating with water/lithium bromide and an aqueous ternary hydroxide, Solar Energy Materials and Solar Cells 63 (4) (2000) 387–399. doi:https://doi.org/10.1016/S0927-0248(00)00058-1.
[64] R. American Society of Heating, A.-C. Engineers, ASHRAE Standard 15: Safety standard for refrigeration systems (2019).
[65] R. Span, Multiparameter equations of state: an accurate source of thermodynamic property data, Springer Verlag, Springer Verlag, 2000. doi:10.1007/978-3-662-04092-8.
[66] W. G. Chapman, K. E. Gubbins, G. Jackson, M. Radosz, SAFT: equation-of-state solution model for associating fluids, Fluid Phase Equilibria 52 (1) (1989) 31 – 38. doi:10.1016/0378-3812(89)80308-5.
[67] W. G. Chapman, K. E. Gubbins, G. Jackson, M. Radosz, New reference equation of state for associating liquids, Industrial & Engineering Chemistry Research 29 (8) (1990) 1709 – 1721. doi:doi.org/10.1021/ie00104a021.
[68] S. Huang, M. Radosz, Equation of state for small, large, polydisperse, and associating molecules, Industrial & Engineering Chemistry Research 29 (11) (1990) 2284 – 2294. doi:doi.org/10.1021/ie00107a014.
[69] M. S. Wertheim, Fluids with highly directional attractive forces. I. Statistical thermodynamics, Journal of Statistical Physics 35 (1984) 19 – 34. doi:doi.org/10.1007/BF01017362.
[70] M. S. Wertheim, Fluids with highly directional attractive forces. II. Thermodynamic perturbation theory and integral equations, Journal of Statistical Physics 35 (1-2) (1984) 35 – 47. doi:doi.org/10.1007/BF01017363.
[71] M. S. Wertheim, Fluids with highly directional attractive forces. III. Multiple attraction sites, Journal of Statistical Physics 42 (3-4) (1986) 459 – 476. doi:doi.org/10.1007/BF01127721.
[72] E. Cea-Klapp, I. Polishuk, R. I. Canales, H. Quinteros-Lama, J. M. Garrido, Estimation of thermodynamic properties and phase equilibria in systems of deep eutectic solvents by pc-saft eos, Industrial & Engineering Chemistry Research 59 (51) (2020) 22292–22300. doi:10.1021/acs.iecr.0c05109.
[73] H. Quinteros-Lama, F. Llovell, J. Wisniak, The polyazeotropic behaviour of the benzene plus hexafluorobenzene system revisited, Journal of Chemical Thermodynamics 113 (2017) 340–349. doi:10.1016/j.jct.2017.07.005.
[74] H. Quinteros-Lama, F. Llovell, Global phase behaviour in carbon dioxide plus *n*-alkanes binary mixtures, Journal of Supercritical Fluids 140 (2018) 147–158. doi:10.1016/j.supflu.2018.06.012.
[75] J. Gross, G. Sadowski, Perturbed-chain SAFT: An equation of state based on a perturbation theory for chain molecules, Industrial & Engineering Chemistry Research 40 (2001) 1244–1260. doi:10.1021/ie0003887.
[76] J. Gross, G. Sadowski, Application of the perturbed-chain SAFT equation of state to associating systems, Industrial & Engineering Chemistry Research 41 (2001) 5510–5515. doi:10.1021/ie010954d.
[77] J. Schilling, J. Gross, A. Bardow, Integrated design of ORC process and working fluid using process flowsheeting software and PC-SAFT, Energy Procedia 129 (2017) 129–136. doi:10.1016/j.egypro.2017.09.184.
[78] K. Parvaneh, A. Rasoolzadeh, A. Shariati, Modeling the phase behavior of refrigerants with ionic liquids using the QC-PC-SAFT equation of state, Journal of Molecular Liquids 274 (2019) 497–504. doi:10.1016/j.molliq.2018.10.116.
[79] DIPPR: The Design Institute for Physical, DIPPE 801 thermophysical property database and DIADEM predictive software (2007).
[80] K. Joback, R. Reid, Estimation of pure-component properties from Group-Contributions, Chemical Engineering Communications 57 (1-6) (1987) 233–243. doi:10.1080/00986448708960487.
[81] J. H. Václav Viňs, PC-SAFT modeling of CO_2 solubilities in hydrophobic deep eutectic solvents, International Journal of Refrigeration 34 (2011) 2109–2117. doi:10.1016/j.ijrefrig.2011.07.002.
[82] A. Groniewsky, C. Wagner, Investigation of the effect of the regenerative heat exchanger on the performance of organic Rankine cycles using perturbed chain Statistical associating fluid theory equation of state, Industrial and Engineering Chemistry Research 59 (44) (2020) 19643–19656. doi:10.1021/acs.iecr.0c03782.
[83] H. Carin, D. Dietz, M. van Osch, G. Kroon, G. Sadowski, M. van Sint Annaland, F. Gallucci, L. F. Zubeir, C. Held, PC-SAFT modeling of CO_2 solubilities in hydrophobic deep eutectic solvents, Fluid Phase Equilibria 448 (2017) 94–98. doi:10.1016/j.fluid.2017.03.028.
[84] J. Lloret, L. Vega, F. Llovell, Accurate description of thermophysical properties of tetraalkylammonium chloride deep eutectic solvents with the soft-SAFT equation of state, Fluid Phase Equilibria 448 (2017) 81–93. doi:10.1016/j.fluid.2017.04.013.
[85] G. S. Lawien F. Zubeir, Christoph Held, M. C. Kroon, PC-SAFT modeling of CO_2 solubilities in deep eutectic solvents, The Journal of Physical Chemistry B 120 (2016) 2300–2310. doi:10.1021/acs.jpcb.5b07888.
[86] D. Jovell, S. B. Gomez, M. E. Zakrzewska, A. V. M. Nunes, J. M. M. Araujo, A. B. Pereiro, , F. Llovell, Insight on the solubility of r134a in fluorinated ionic liquids and deep eutectic solvents, Journal of Chemical Engineering Data 65 (1-6) (2020) 49564969. doi:10.1021/acs.jced.0c00588.
[87] S. E. Quiñones-Cisneros, Barotropic Phenomena in Complex Phase Behaviour, Physical Chemistry Chemical Physics 6 (9) (2004) 2307 – 2313. doi:10.1039/b316123d.
[88] H. Quinteros-Lama, G. Pisoni, J. M. Garrido, A. Mejía, H. Segura, Barotropic Phenomena in Binary Mixtures, Fluid Phase Equilibria 394 (2015) 175 – 185. doi:10.1016/j.fluid.2015.03.004.